A CFD VALIDATION STUDY USING ARTEMIS 1 ORBITAL SLOSH TEST DATA

Dr. Jedediah M. Storey*

Advancements in liquid propellant management science and technologies are key to increasing safety, decreasing cost, and increasing payload mass of NASA space missions. Liquid propellant usually comprises a large portion of the total mass of launch vehicles and spacecraft, so predicting and controlling the motion of it are important. Computational fluid dynamics (CFD) programs are critical to predicting slosh dynamics, but CFD programs require experimental validation with physically relevant test data before the results can be trusted. Low-gravity slosh test data is lacking, and most of what exists is inadequate for CFD validation. A potential slosh risk for Orion, and the lack of validated low-gravity slosh models, led to performing on-orbit slosh tests during the Artemis 1 mission to assess the impacts of slosh on the guidance, navigation, and control of Orion. This work details the validation of a coupled slosh-motion CFD model using the Orion orbital slosh test data set.

INTRODUCTION

Foreword

This paper is a condensed version of an appendix from a NASA NESC Report titled "Artemis II MPCV/ICPS Separation Analysis" (in review). All sensitive information in the original report has been redacted for the current paper. Numbers have been removed from plot y-axes. Many of the original references are not publicly available, and some have been replaced with publicly available websites that contain the information being cited. DFTO2 results are not presented due to the paper length limit.

Background: Low-G Slosh

Because liquid propellant usually makes up a large portion of the total mass of launch vehicles and spacecraft, advancements in liquid propellant management science and technologies are key to increasing safety, decreasing cost, and increasing payload mass of space missions. The fluid dynamics of liquid propellants in an accelerated environment, such as on a planetary body or while a space vehicle is thrusting, are different than in a low acceleration environment, i.e. low-gravity (low-G) or microgravity.[1] Computational Fluid Dynamics (CFD) has been used extensively to simulate and predict propellant slosh, despite not being properly validated for microgravity environments. Several rocket and spacecraft mishaps have caused the validity of CFD slosh predictions to be questioned.[2,3] For slosh simulations, CFD validation typically consists of comparing test and simulation liquid distributions, forces, and/or moments. For coupled slosh-body motion, where the slosh dynamics influence the motion of the space vehicle, CFD validation can be accomplished by comparing simulated and test motion (e.g. accelerations and rotation rates). Ground slosh data exists in the

* Thermal-Fluid Discipline Expert, LSP Environments and Launch Approval Branch, Kennedy Space Center

scientific literature and industry for a multitude of tank shapes and fluids, and CFD programs have been validated using these data. However, more low-G slosh data needs to be collected and used to validate CFD.

Two important nondimensional numbers for the characterization of slosh are the Bond number (Bo) and Weber number (We), given by Equations (1) and (2), respectively.*

$$Bo = \frac{body\ acceleration\ forces}{surface\ tension\ forces} = \frac{\rho a R^2}{\sigma} \tag{1}$$

$$We = \frac{inertial\ forces}{surface\ tension\ forces} = \frac{\rho R V^2}{\sigma} \tag{2}$$

Where a is acceleration, R is characteristic length (tank radius in this work), V is liquid velocity, ρ is liquid density, and σ *is* surface tension. For the purposes of this work, "high-G" is defined to be $Bo \gtrsim 100$, "low-G" $Bo \lesssim 100$, and microgravity to be $Bo \lesssim 1$. Low We microgravity, i.e. $We < 1, Bo < 1$, slosh is characterized by slow surface waves with an unchanging liquid configuration. On the other hand, high We ($We >> 1$) microgravity ($Bo < 1$) or low-G ($Bo \lesssim 100$) slosh is often characterized by drops and blobs of liquid moving around the tank. These nondimensional number "regimes" help identify the physical relevance of a slosh data set to a specific application.[4] For example, a CFD simulation validated with high-G slosh data should not be used to predict microgravity slosh without additional validation with microgravity slosh data because the fluid dynamics of high-G slosh are different than for microgravity slosh.

Orion Overview

The primary components of Orion are a crew module (CM) and European Service Module (ESM). A crew module adapter (CMA) connects the ESM and CM. The ESM has four solar arrays, four propellant tanks and a variety of thrusters. Figure 1 is a picture of Orion in its flight configuration.†

Figure 1. Rendering of Orion in Flight Configuration

* See the Notations table near end

† NASA Render, https://www.flickr.com/photos/nasaorion/50942526198/in/album-72157633479431041/

Orion Slosh Tests Overview

Errant accelerations from slosh are a risk to Rendezvous Proximity Operations and Docking (RPOD) operations. For example, during docking, two spacecraft begin stationary relative to each other, then one performs a brief acceleration burn to close the distance followed by a brief deceleration burn to reduce impact. The acceleration-deceleration can disturb propellant in the tanks, and, if the propellant mass fraction is high enough, can cause significant, undesirable acceleration in the direction of the docking target. Orion was determined to be subject to a similar risk.[5]

The Orion Guidance, Navigation, and Control (GNC) team proposed an on-orbit developmental flight test objective (DFTO) to observe the effects of slosh from an axial reaction control system (RCS) burn. NASA and contractors designed the DFTO slosh test for the uncrewed Artemis 1 mission.[5] The test was performed twice during the mission, once after outbound powered flyby (OPF) and once after return powered flyby (RPF).

Objectives

The objectives of this work are:

1. Confirm the hypothesis that an anomalous acceleration signal was due to slosh.
2. Determine the cause of a timing discrepancy between CFD from the planning stages of the DFTOs and reality.
3. Validate a coupled body-slosh motion CFD simulation with the Orion slosh DFTO data.

ORION VEHICLE DETAILS

Propellants

The ESM thrusters use mixed oxides of nitrogen (MON) as an oxidizer and monomethylhydrazine (MMH) as a fuel. Gaseous helium (GHe) is used as a pressurant. The service module (SM) propellant mass at launch can be >30% of the total on-orbit spacecraft mass.[*] Tank temperatures and pressures during the DFTOs were used to calculate liquid and ullage gas properties. The liquid and gas phases are assumed to be incompressible for the simulations. Itis assumed that the propellant burned during the DFTOs is negligible, so the simulations do not include propellant outflow.

The static, advancing, and receding contact angles of MON and MMH on the tanks' material, titanium, are near 0 degrees.[6] An arbitrary value near 0, 0.1 deg, was selected as a constant contact angle for the simulations. Given the resolution of the simulation mesh, it is likely that any values < 1 deg would give similar results.

Thrusters

The ESM has a Shuttle-derived orbital maneuvering system engine (OMS) for its main engine. It has eight auxiliary thrusters that provide backup to the OMS and thrust for abort and orbit/trajectory correction maneuvers. It has twenty-four RCS thrusters for redundant attitude control, rendezvous maneuvers, and small trajectory corrections.[†] Twelve of the RCS thrusters were used for DFTO1 and DFTO2. The large OMS was not used for the slosh tests, partially for safety, but also because the OMS results in an acceleration in the high-G regime, and high-G slosh was not a goal of the slosh DFTOs. Minimizing the ΔV perturbation to the Orion trajectory by applying a counter-burn at the end of the test was desired. The auxiliary thrusters were not used because all eight thrust in the same direction, while the RCS has thrusters in all directions, making the RCS thrusters preferable. The RCS thrusters have a nominal thrust of about 220 N.[†] Individual thruster performance was obtained from References 7, 8, and 9. Like all thruster systems, their thrust was dependent on the inlet propellant pressure and temperature. Reference 8 contains thruster ID, position, point-of-action, and thrust direction for all RCS thrusters in the Spacecraft Structural Coordinate System.

[*] https://directory.eoportal.org/satellite-missions/artemis-i#nasas-deep-space-network
[†] https://www.esa.int/Science_Exploration/Human_and_Robotic_Exploration/Orion/Propulsion

All thrusters have a startup and shutdown transient. Information from References 9 and 10 were used to create the startup and shutdown transients for the ESM RCS thrusters. The timing of the startup transient was adjusted shorter because that resulted in the accelerations and/or rotation rates having a better match to flight data. A python script was written to generate a thrust vs. time table for each thruster in a format that the simulation software can read. Nominal characteristics for each thruster are inputs. The nominal thrusts are corrected for inlet conditions. Mass flowrate is calculated from nominal specific impulse, I_{sp}, and adjusted thrust, T, for each thruster using Eq. (3).

$$\dot{m} = \frac{T}{I_{sp} * 9.80665} \tag{3}$$

Transient thrust is then calculated using Eq. (4).

$$T(t) = \left(I_{sp,t}(t) + (I_{sp} - I_{sp,t,steady})\right) * 9.80665 * \dot{m} \tag{4}$$

where $I_{sp,t}$ is the Isp transient array and $I_{sp,t,steady}$ is the steady state Isp from the Isp transient array. This transient thrust is then interpolated with 1D cubic interpolation (scipy's pchip) to a time step of 0.001 s and spliced into the thruster's open loop firing pattern (see DFTO Maneuver Description). It is understood that the way the thrust transient was modeled is an approximation of reality.

Coordinate Systems

The relevant coordinate systems for this work are the SM, Spacecraft Structural, and Orion Body coordinate systems. These were included in the simulation so that they could be referenced by various simulation components without having to manually transform all inputs into the same coordinate system. The exact definitions of these coordinate systems[10] has been redacted. The "X" axis is along the CM+ESM axis, and "Y" and "Z" are defined relative to features on Orion. CAD of the tanks was used to determine their origins and geometric centers in the various coordinate systems.

Propellant Tank Details

The ESM propellant tanks are pill shaped, approximately 1.1 m diameter and 2.5 m long.[*] There are four propellant tanks, one "upstream" tank and one "downstream" tank for each propellant. All of the tanks have the same walls, but the internals differ between upstream and downstream tanks. Pictures of these tanks are available online.

The upstream tanks contain an anti-vortex baffle (AVB) in the sump, a barrel-shaped set of baffles in the forward half of the tank, and a gas diffuser in the forward end. The downstream tank volume is bifurcated by a cone. The internals are designed to retain liquid in the aft compartment so that the sump is always wetted. The forward compartment contains an AVB in the cone and a gas diffuser in the forward end. Pictures of the CAD and simulation geometry have been redacted.

Mass Properties

Accurate simulation of Orion's dynamics required accurate knowledge of its mass properties. Tables 2, 3, and 7 of Reference 11 are the primary source for Artemis 1 mass properties for this work. The data is presented in the Spacecraft Structural Coordinate System with inertias about each component's CG. The assembly CG was calculated and used with the parallel axis theorem to sum the component inertias, resulting in a single rigid body mass, CG, and inertia tensor. Mass properties have been redacted.

Several assumptions were made to make mass properties determination simpler. It was assumed that the CM remains in its liftoff configuration, i.e. it did not expend any of its propellant. The downstream ESM tanks were full for DFTO1; it was assumed that the propellant in those tanks was solid, so the propellant was included in the rigid body's mass properties. In reality, the inertia of propellants does not couple perfectly with the moving body. To understand this, one can imagine a full tank located near the spin axis of a spacecraft initially not spinning. As the spacecraft spins up, the liquid in the tank initially does not spin. It takes time for viscous drag from the spinning wall and pressure drag from features inside the tank to transfer momentum to the liquid. The SM's tanks are not located near rotation axes, and Orion rotation rates for the slosh

DFTOs were low, so the assumption of perfect inertial coupling (solid propellant) is more valid than in the given hypothetical example. The upstream tanks' propellants were simulated for DFTO1, so they were not included in the rigid body's mass properties. The SM inertia used assumed the solar arrays were fully deployed. Aside from their mass and inertia, the solar arrays were not modeled.

Multiple simulations of DFTO1 were run to determine the sensitivity of the resultant accelerations and rotation rates to CG and inertia variations *within their published uncertainties*. Y and Z rotation rates, and therefore orientation versus time, were found to be hypersensitive to Z and Y (respectively) CG variations. The DFTO1 and DFTO2 Y and Z CGs incorporate small shifts because these resulted in a large improvement in simulation-test data agreement for the Z and Y rotation rates. It was found that the accelerations and X rotation rate were relatively insensitive to CG variations, and all accelerations and rotation rates appeared to be relatively insensitive to inertia variations.

Orion IMUs

Orion had three inertial measurement units (IMUs).[10] These provide 3-axis accelerations and 3-axis rotation rates in their local coordinate systems. Only data from one IMU was recorded at any given time, with the other two acting as backups. The "Navigation Center of Computation" (CC), which is the point of interest in these IMUs, is calculated in the Spacecraft Structural Coordinate System.

The test data from these IMUs were rotated into the Orion body frame, but the origin was kept at the OIMU CCs. The CC location vectors were input into the simulation and used to perform kinematic transformations of the body accelerations, which are calculated by the simulation in the Orion Body Frame about the rigid body CG, to the OIMUs' CCs. Eq. (5) is the acceleration transformation equation.[12] If the acceleration, $\boldsymbol{a}_{O'}$, at a point, O', and the body's angular velocity, $\boldsymbol{\omega}$, are known, then the acceleration, $\boldsymbol{a}_P$, at the point of interest, *P*, in the rigid body is

$$\boldsymbol{a}_P = \boldsymbol{a}_{O'} + \dot{\boldsymbol{\omega}} \times \boldsymbol{r'}_P + \boldsymbol{\omega} \times (\boldsymbol{\omega} \times \boldsymbol{r'}_P) \tag{5}$$

where $\boldsymbol{r'}_P$ is the position vector of the point, *P*, relative to O'.

The acceleration transformation was necessary despite the small rotation rates due to how small the accelerations of interest were. The simulation accelerations were transformed to the OIMU2 CC location instead of transforming the test accelerations to the rigid body CG (origin of Orion body frame) for several reasons: 1. Body angular acceleration is necessary for performing the transformation and was directly available in the simulation. The noisy angular velocity test data would have to be differentiated to obtain angular acceleration in order to transform the test accelerations, and differentiation tends to amplify noise. 2. The acceleration test data is very noisy, and transforming it would have increased the noise. Conversely, the simulation data had far less noise (numerical only), so was the better choice for transforming.

DFTO MANEUVER DESCRIPTION

Orion performed the same basic open-loop maneuver for both slosh DFTOs.[5] First, Orion free-drifted with no thrust events for 10 minutes. Next, the four aft-firing RCS thrusters fired for 10 s resulting in +X acceleration. Then Orion coasted (free-drift) for 120 s. Finally, the four forward-firing RCS thrusters fired for 10 s resulting in -X acceleration. The second burn was done to cancel the ΔV from the first burn so that the DFTO would not impact the overall trajectory. Some balancing thrusters were used to null rates during the 10 s X burns, but they were not used during the free-drift before or between X thrust events. The firing pattern for the balancing thrusters was created using an anticipated CG.

Maneuver Initial Condition

Fluid surface energy is a combination of acceleration energy and surface tension energy, and it is affected by boundary conditions, e.g. boundary shape and contact angle. The fluid surface will tend to rearrange to achieve a minimum energy configuration, i.e. surface energy is minimized at equilibrium. Tanks can have one, multiple, or infinite minimum energy surfaces, and therefore steady fluid configurations, depending on numerous factors.

The free-drift prior to thrust initiation allows the propellant to come to a steady state prior to the +X burn. The fluid configuration at this time will be referred to as the "initial condition" for the simulation. Although the exact fluid configuration after the free-drift is unknown due to the lack of a camera or propellant monitoring hardware in the tanks, the geometry of the upstream tank and its internal hardware, the fill level, and the fact that the fluids are wetting, make it likely that there is one minimum-surface-energy fluid configuration for DFTO1, which will be achieved given sufficient time. There are three main ways of estimating this initial condition: 1. Engineering judgement, 2. A surface energy solver, 3. CFD. A detailed discussion of how the initial condition was found with CFD in this work is discussed in CFD Setup and Execution.

The team that designed the DFTO maneuvers used CFD to predict the initial condition at the start of the +X burn.[5] Specifically, the team used Flow-3D with a tank geometry that did not include internal baffles. This simulation predicted a centered ullage bubble, which is the minimum surface energy fluid configuration for a pill-shaped tank partially filled with a wetting liquid. The team used that initial condition to run simulations to help design the DFTO maneuvers. This is how 10 s X burn was selected: according to these simulations, X-axis excitation would provide the highest slosh forces (and be most relevant to a RPOD maneuver), and the liquid in the forward dome would take more than 10 s to traverse the axis of the tank and impact the aft end of the tank, so cutting off the thrusters at 10 s would allow for measurement of Orion motion due to slosh without the thruster effects. Unfortunately, as will be shown in the Results Section, the slosh wave impacted the aft end of the tank while Orion was still under thrust.

Thruster Schedule

Tables from Reference 13 give the RCS thruster firing patterns for DFTO 1 and 2. The transient startup profile was spliced into the off-on transitions using the python script mentioned in previously. The thrust versus time profile for each thruster was then output in a format that the simulation could read.

CFD SETUP AND EXECUTION

This section discusses the setup and execution of the CFD cases that were run as part of this work. The CFD simulation software used was Siemens STAR-CCM+ [14]. The tank details and geometry are discussed in Section Orion Vehicle Details; this geometry was imported into STAR-CCM+ for meshing. Two classes of CFD cases were run: "simplified" and "detailed". The simplified cases used smooth tank walls with no internal geometry (e.g. baffles). The detailed cases included the internal geometry. All images of the mesh and simulation results have been redacted.

Mesh

Pointwise[15] was used to create structured meshes for the simplified geometries. Structured meshes only have hexahedral cells. All cells were high quality (max equiangle skewness < 0.53). The upstream tank's mesh count was approximately 34,000. The downstream tank's mesh count was approximately 38,000.

Creating a structured mesh with the internal baffles would have been too difficult. Instead, STAR-CCM+'s Automated Trimmer (hexahedral) and Prism Layer Meshers were used to generate meshes for the detailed geometries. The upstream tank's mesh count was approximately 1.34M. The downstream tank's forward compartment mesh count was approximately 1.26M. The aft compartment was not meshed. The meshes were hexahedral-dominant and cells were concentrated on and near boundaries because accurately modeling surface tension was important for these cases. Pictures of the detailed meshes are omitted due to proprietary geometry.

Setup and Settings

After the tank was meshed, the physics were setup. The following is a subset of the final simulation settings:

- Coordinate systems for SM, spacecraft structural, and Orion body
- Adaptive time stepping based on CFL (Courant–Friedrichs–Lewy convergence condition number) and free-surface CFL
- Implicit unsteady with second-order temporal discretization

- Laminar
- Two-phase, second-order Volume-of-Fluid (VoF) with HRIC
- Surface tension VoF phase interaction, constant contact angle
- Second-order segregated flow solver
- Dynamic fluid body interaction (DFBI) 6 degree-of-freedom (6DoF) solver
- Orion non-sloshing mass defined as a free motion DFBI body with mass and inertia
- Custom field functions for kinematic transformation of CG body acceleration to the OIMU locations
- Custom field functions for calculating fluid CGs and inertias
- 2D baffle surfaces in the detailed geometry were set as internal boundaries (walls)

The DFBI 6DoF solver applies acceleration and rotation rates to the fluid regions, and the resultant fluid forces and moments are applied to the body for each time step. The 12 thrusters were modeled as propulsion forces, the inputs for which were a location of thrust application, thrust level, and direction of the thrust. Thrust level was controlled by an imported and internally linearly interpolated table for each thruster.

Initial Conditions

First Simulations.

The exact fluid configuration after the free-drift is unknown due to the lack of a camera or propellant monitoring hardware in the tanks. The geometry of the upstream tank and its internal hardware, the fill level, and the fact that the fluids are wetting, make it likely that there is one minimum-surface-energy fluid configuration for DFTO1, which will be achieved given sufficient time. The fluid configuration at the end of the free-drift will be referred to as the "initial condition" for the CFD simulation of the DFTO maneuver, but that had to be found via another CFD simulation first.

If only one minimum-surface-energy fluid configuration exists for the reasons mentioned previously, the initial fluid configuration for these first simulations should only affect the amount of simulation time it takes to achieve that minimum-surface-energy state, not the final state itself. A pill-shaped (hemisphere-cylinder-hemisphere) initialization object representing a centered ullage "bubble", with diameter equal to the tank diameter, was used to initialize the gas and liquid locations for the first simulations. The initialization object was centered axially so that half of the liquid was on each end of the tank. Flat (plane perpendicular to tank axis) fluid interfaces would have been a better initialization choice for a contact angle of 90 deg, but a pill-shaped gas bubble is a better choice for small contact angles because it decreases the amount of time it takes for the first simulations to achieve a steady final state because the pill-shape is closer to the final state's gas bubble shape. The lengths of the cylinder portions of the initialization objects were manually tuned to achieve as close to the desired liquid masses (best estimate of actual) as possible. It is assumed that the achieved masses are close enough to the desired masses to not affect the results.

The first simulations were run with first-order temporal discretization, a rotating reference frame, and a frozen DFBI solver until steady state was achieved. First-order temporal discretization was used for stability and because accurate time history was not required for these first simulations. Orion did not perfectly null out rotation prior to initiating free-drift. The rotating reference frame modeled the small average angular velocity that Orion experienced during its free-drift prior to the DFTO maneuvers without spending the computational effort of actually rotating the body with the DFBI motion solver. A Bo << 1 at this time indicates that the surface tension forces were dominant. The final steady fluid configuration "initial condition" was stored in a STAR-CCM+ construct called a data mapper.

The simulation was then copied to a new file and reset to 0 s. The data-mapped initial condition was used to initialize velocity, pressure, and volume fraction for the current, DFTO maneuver simulation. Temporal discretization was set to second order, the rotating reference frame was deactivated, the DFBI solver was unfrozen, and DFBI initial angular velocity equal to the free-drift angular velocity was applied. The thruster tables had a 5 s delay before the +X burn built-in to allow the simulation to stabilize.

Initial Conditions for the Maneuver Simulations.

The DFTO1 simplified simulation had a centered ullage bubble initial condition. The DFTO1 detailed simulation initial condition had a large portion of the liquid that would have been in the forward dome gathered around the baffles, which shifted the propellants' CGs aft (-X) compared to the no-baffle case.

Simulation Fluid Film.

In a tank partially filled with a wetting liquid in microgravity, capillary forces cause a thin fluid film to cover the portions of the inside wall that are not covered in bulk liquid.[16] The VoF scheme attempted to resolve the fluid film without enough mesh resolution to do so, resulting in a low volume fraction in the wall cells that occasionally went over 0.5 (50%). Because the fluid isosurface isovalue is nominally set to 0.5, the fluid surface gets rendered in these wall cells, but not wall cells with volume fractions less than 0.5, resulting in patches of fluid surface instead of a complete film. Rendering the fluid surface at an isovalue of 0.01 instead of 0.5, i.e. rendered if more than 1% of the cell volume is liquid, shows a complete, albeit too thick, film. A fine enough mesh to resolve the fluid film would have been computationally prohibitive. There are fluid film models that *model* the fluid film instead of resolving it. STAR-CCM+ has a fluid film model that is compatible with VoF, but it is not compatible with DFBI, and it severely limits CFL and time step, so it was not used. It is assumed that the results were not significantly impacted by not fully resolving the wall fluid film. This is a decent assumption when surface tension forces do not dominate the fluid dynamics, i.e. for systems dominated by inertial or acceleration forces, which is the case for these tanks around the times of the anomalous accelerations of interest.

CFD Execution

Adaptive time step mean-CFL limit was set to 0.5, max CFL limit was kept around 3-5, and free surface CFL limit at 0.5. This resulted in a time step of approximately 0.0001 – 0.002 s in the detailed simulations. The simplified simulations were typically not CFL limited due to having a large minimum cell size. Residuals and mass imbalance were monitored for to check/ensure convergence.

Aggressive VoF time stepping was used at the suggestion of Siemens. The basic idea is to use smaller time steps, higher under relaxation factors, and lower algebraic multigrid (AMG) tolerance to drive the number of iterations/time step as low as possible. The smaller time steps result in better time accuracy and the reduction in iterations reduces the penalty from using smaller time steps. This was easier to achieve in simulations using the higher quality simplified mesh than the detailed mesh.

Execution time for each simplified simulation was on the order of hours when run on a 16-core workstation. Execution time for each detailed simulation was 1-2 weeks when run on 120 cores of Launch Services Program (LSP) Fluid's compute cluster while scene rendering occurred on a workstation with a graphics processing unit (GPU). Execution speed is why the simplified simulations were run: the shorter turnaround time allowed for rapid iteration and testing of simulation settings that could then be applied to the detailed simulations.

RESULTS

Test and simulation data were post-processed and plotted in MATLAB[17]. All y-axes have had numbers redacted.

Test Data Filtering

The signal-to-noise ratio of the OIMU data was poor, not because the IMUs underperformed, but because the signals of interest were small. The accelerometer data's signal was below the random noise amplitude. Although lowpass filtering yielded decent results, the use of a local regression smoother, "lowess" in MATLAB, yielded better results. A lowpass filter will retain noise frequency content below and around the cutoff frequency. When applied to a very noisy signal, this can result oscillations superimposed on the signal of interest that may or may not be real. In contrast, lowess tends to reduce the amplitude of some frequency content up to a threshold, beyond which it reduces the amplitude to near 0. The lowess smoother seemed to work better than a moving average, likely for the same reason because a moving average is a type of finite impulse response (FIR) lowpass filter. The gyroscope data was generally less noisy, with the signal above the noise amplitude, and the noise was primarily high frequency. Thus, the rotation rates were filtered with a

high-order lowpass 4 Hz stopband frequency infinite impulse response (IRR) filter applied with filtfilt for zero-phase distortion.

Data commentary in this section is limited to the topics of filtering and noise. Only the +X thrust event from DFTO1 is presented for sake of brevity. Figures 2 and 3 shows the unfiltered and filtered DFTO1 test data in the Orion Body Frame at the OIMU2 origin. The dark "filt" curves are the lighter-colored raw data filtered as described above.

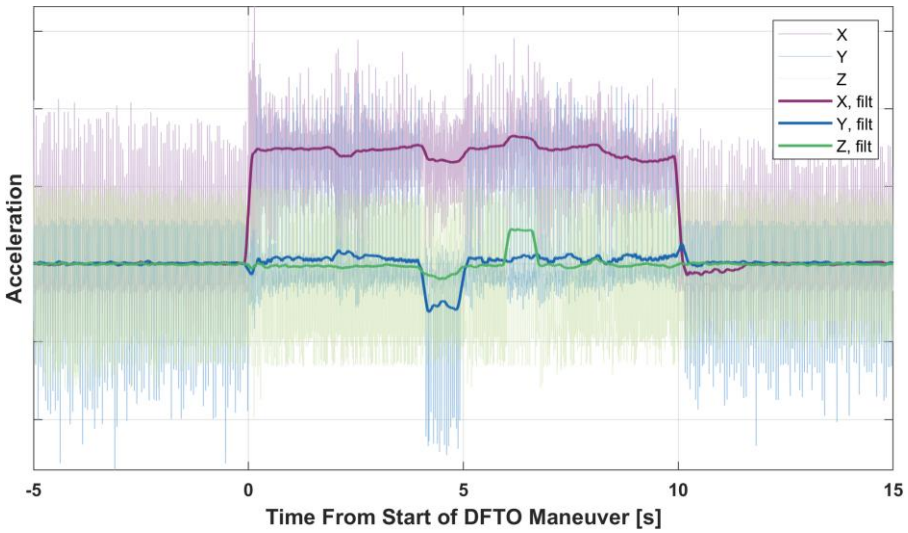

Figure 2. Unfiltered vs. Filtered DFTO1 Acceleration Data, +X Thrust Event

Figure 2 shows that some noise remained after smoothing, but more smoothing would have resulted in unacceptable smearing and signal loss. The step-like bumps are from balancing thrusters firing, but many of the small bumps and oscillations are likely noise. However, due to their magnitude, the -Y bump at +X thrust initiation and +Y bump at +X thrust termination are likely not noise. Balancing thrusters were not firing during thrust termination, so the +Y bump then cannot be due to a Y thrust component.

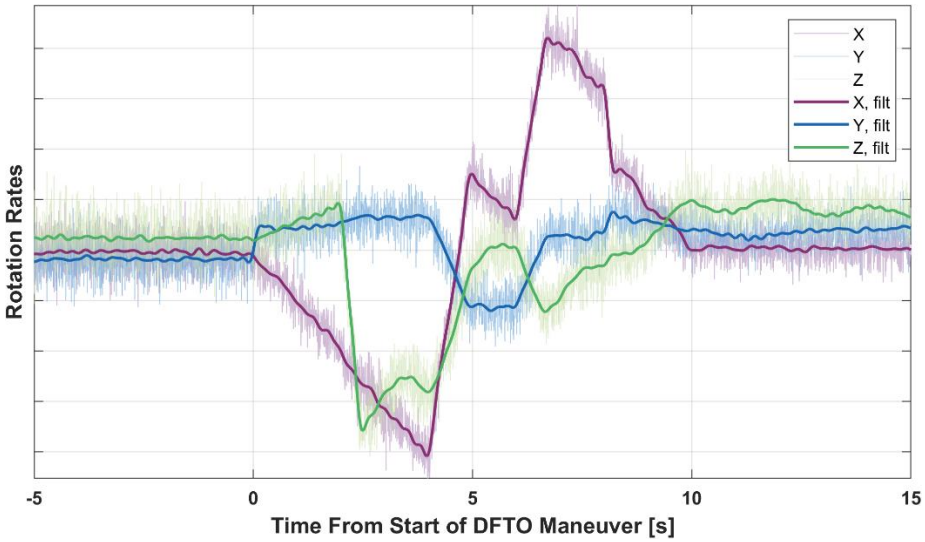

Figure 3. Unfiltered vs. Filtered DFTO1 Rotation Rate Data, +X Thrust Event

A 4 Hz stopband was high enough to leave the primary solar array flex mode (≈0.46 Hz) frequency content in the signal, which can be seen in the Z rotation rate in Figure 3 after stopping X thrust.

Simulation Results

This section presents the simplified and detailed CFD simulations results for DFTO1. The simplified simulation was used to test CFD settings and check the effects of varying inertias and CG within their uncertainty bounds. The simplified simulations always had excellent convergence, no significant numerical noise, and the results did not require filtering. Execution speed in the detailed simulation was pushed right to the limit of acceptable convergence based on residuals, mass imbalance (continuity), and fluid force (momentum) noise. There was some low-amplitude, high-frequency numerical noise and occasional noise spikes in the accelerations, forces, and moments that required lowpass filtering in post-processing. When the numerical error/noise was deemed large enough to have affected the simulation results, the simulation was restarted from an earlier time point with adjusted settings to improve convergence.

DFTO1 Simplified Simulation.

Figures 4-6 are plots of the DFTO1 simplified simulation accelerations compared to the test data in the Orion Body Frame at the OIMU2 origin.

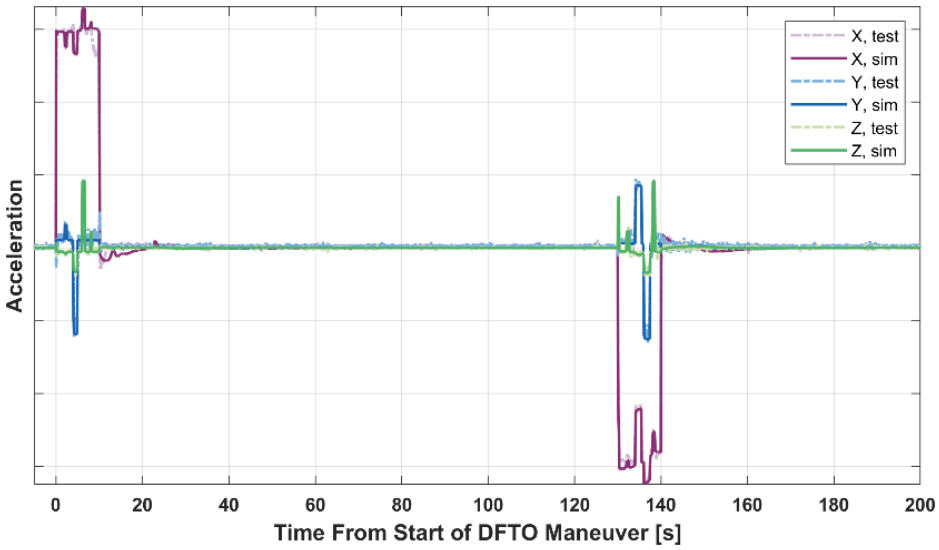

Figure 4. DFTO1 Simplified Simulation vs. Test Data: Accelerations

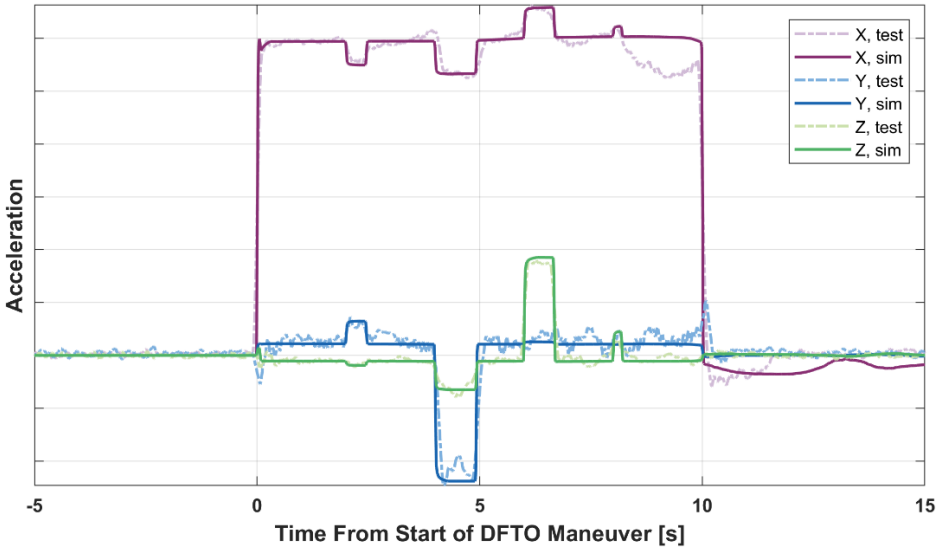

Figure 5. DFTO1 Simplified Simulation vs. Test Data: Accelerations, +X Thrust Event

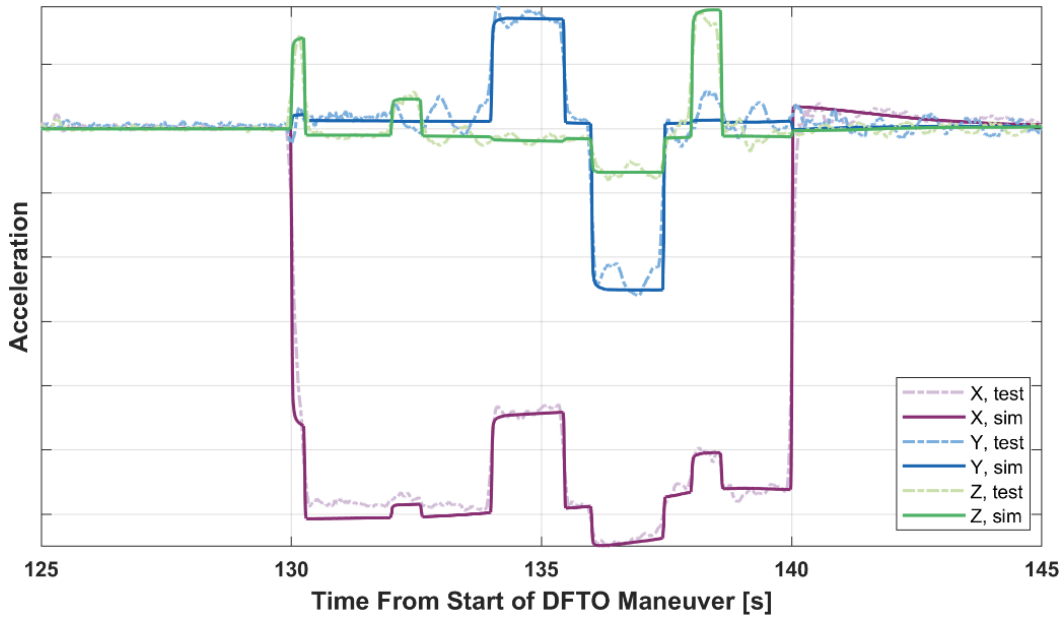

Figure 6. DFTO1 Simplified Simulation vs. Test Data: Accelerations, -X Thrust Event

The simplified simulation reproduced the rigid body motion effects well. The -Y bump at +X thrust initiation and +Y bump at +X thrust termination in Figure 5 were not reproduced in the simulation. The roughly 1 Hz oscillation in the Y acceleration visible in Figure 5 and Figure 6 was also not reproduced by the simulation. The other major test data feature in Figure 5 that was not reproduced by the simulation is the dip in X acceleration starting around 8 s and subsequent rise to 0 acceleration after 10 s, which are hypothesized to be due to slosh. After the initiation of +X thrust, the simulation videos show an annular slosh wave traveling along each tank wall from the forward dome towards the aft dome. The liquid clung to the walls due to surface tension, which was why the wave is annular rather than a single slug of liquid traveling down the tank axis. This wave enters the aft dome around 9.5 s, with the bulk of the wave having impacted by 14 s. This explains the small dip in acceleration just prior to the thrusters cutting off, as well as the -X acceleration after the thrusters cut off. The annular slosh wave was funneled radially inward by the aft dome, forming a geyser that traveled along the tanks' centerlines towards the forward dome. The small peak in simulation +X acceleration around 25 s in Figure 4 is from the geyser impacting the forward dome. The test data does not show evidence of a geyser impact. The timing of the slosh events was slightly different between the two tanks due to their position in the ESM and differences in fluid properties; specifically, MMH tended to lag MON. The slosh proceeded to mostly damp out before the -X thrust event at 130 s, though it did not have time to reach the steady initial condition. Instead, the simulated liquid distribution at 130 s was more evenly distributed along the walls. The -X thrust accelerated the liquid that is in the aft dome at 130 s towards the forward dome, mostly along the tank walls. Because the liquid was not concentrated in the aft dome, it did not form a distinct slosh wave as it did for the +X thrust event; instead, the migration to the forward dome was more continuous. The forward liquid motion damps out after thrust termination at 140 s, and Figure 6 simulation X acceleration shows a decrease from small positive acceleration to 0 during this time. It is difficult to distinguish from noise, but the X acceleration in the test data also appears to have the same trend after 140 s. Although it is unlikely that the accuracy of this simulation was enough to reproduce the precise distribution of liquid in the real tanks at 130 s, the +X thrust event coupled with 120 s of free drift likely resulted in a semi-evenly distributed wall-bound liquid distribution at 130 s, similar to what was seen in the simulation. Then the -X thrust event caused similar forward liquid motion, culminating in a similar positive acceleration tail after 140 s.

Figures 7-9 are plots of the DFTO1 simplified simulation rotation rates compared to the test data in the Orion Body Frame.

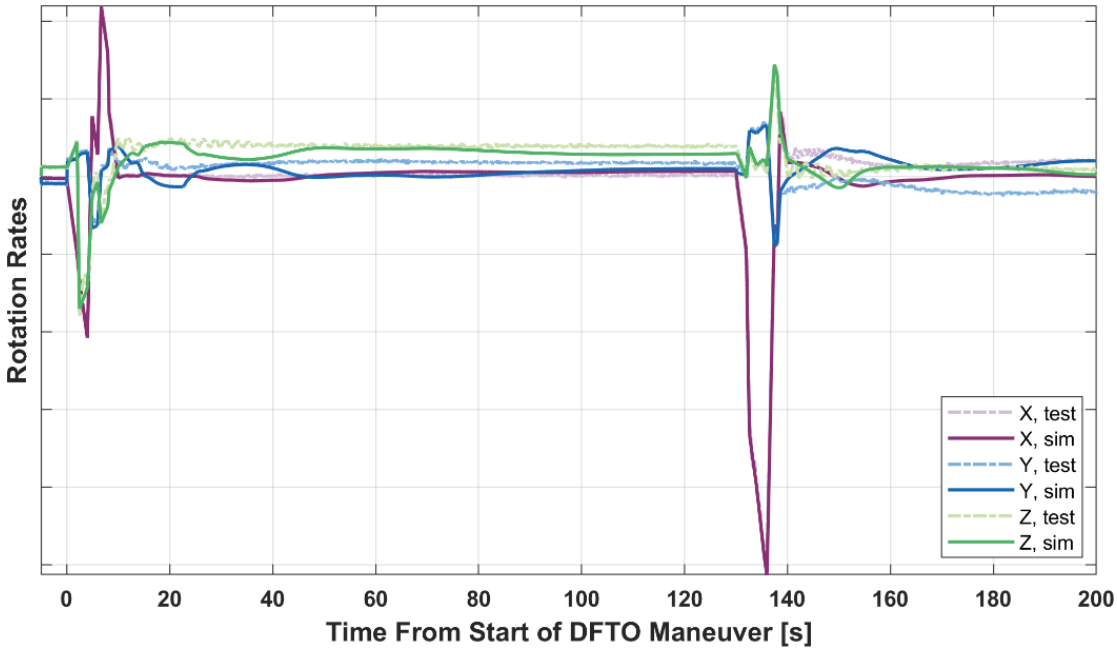

Figure 7. DFTO1 Simplified Simulation vs. Test Data: Rotation Rates

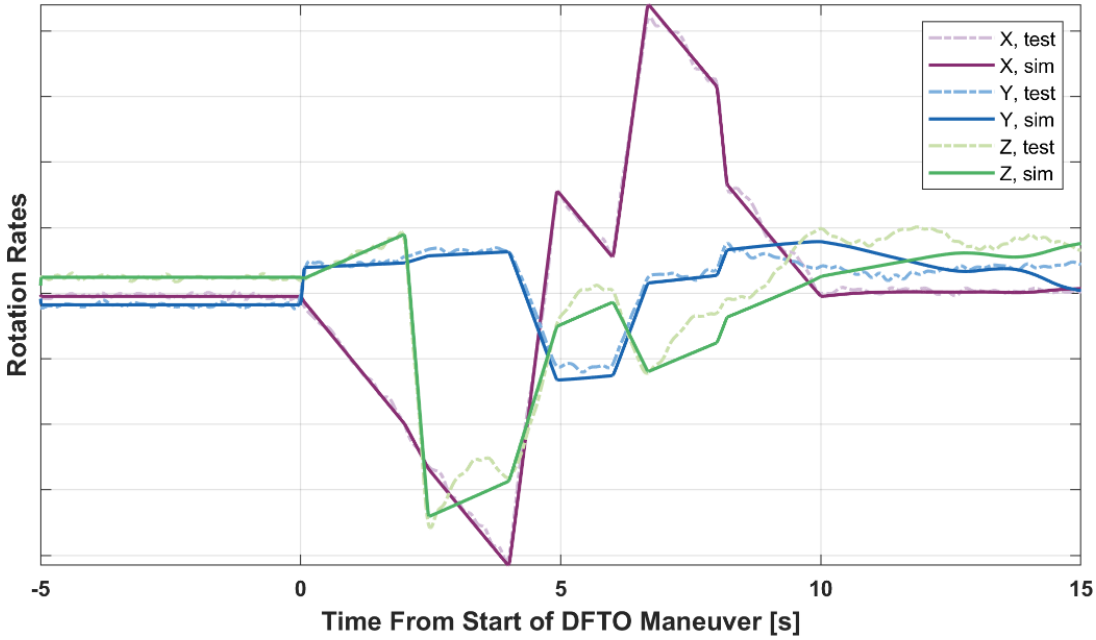

Figure 8. DFTO1 Simplified Simulation vs. Test Data: Rotation Rates, +X Thrust Event

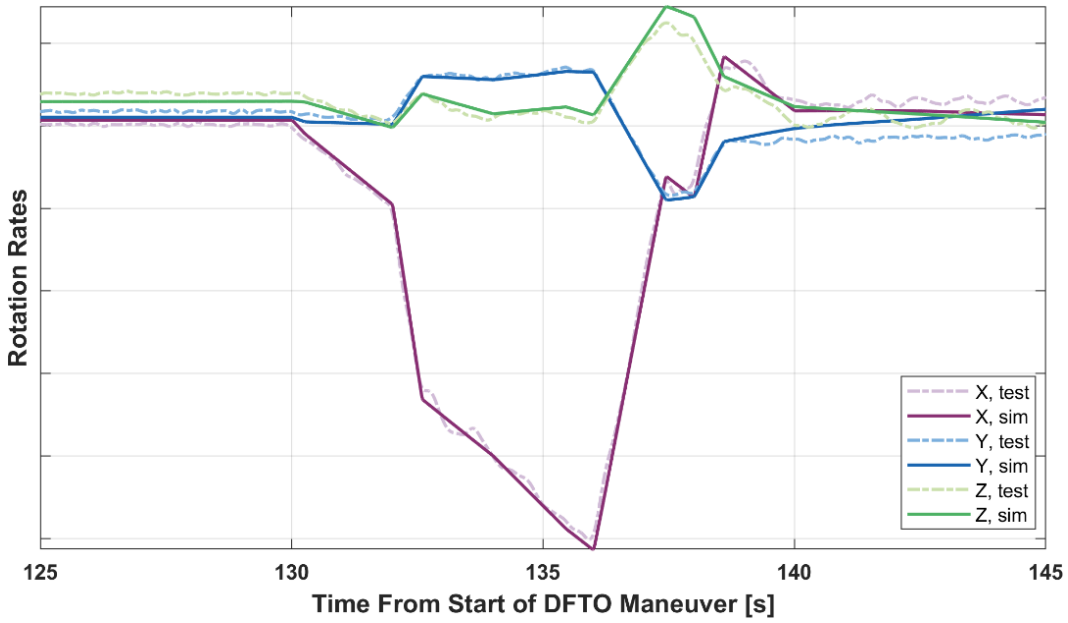

Figure 9. DFTO1 Simplified Simulation vs. Test Data: Rotation Rates, -X Thrust Event

Roll rates were not perfectly nulled prior to the free drift before 0 s, nor after the X thrust events, so some rotation remained during the 120 s free-drift and after the +X thrust event.

As expected, the primary solar array flex mode (≈0.46 Hz) visible in the Z rotation rate test data in Figure 7 after X thrust termination was not reproduced by the simulation. This mode shows up in the Z rotation rate despite the solar arrays being geometrically symmetric because the spacecraft's CG for DFTO1 was offset from geometric center in +Y. This offset caused asymmetric array flexing and cyclic Z torque triggered by the rapid removal of X acceleration. The +Y CG offset coupled with a steady +X thrust caused a steady +Z torque, which can be seen as a positive slope in the Z rotation rate curve in Figure 8 when no balancing thrusters are active. The opposite can be seen during -X thrust in Figure 9. The X roll, which was primarily what the balancing thrusters were correcting, was due to a moment produced by all four thrusters used to produce the +/- X thrust acting on off-axis point-of-action offsets. The X roll rate magnitude was higher during the -X thrust event because the balancing thruster firing pattern was different.

The solar array flex mode is responsible for the test data Z rotation rate humps above the simulation Z rotation rate around 3, 5.5, and 7 s in Figure 8. There is an approximately 1 Hz mode visible in the X rotation rate test data in Figure 9 that was also not reproduced by the simulation; the cause of this is unknown, but given the location of OIMU2 relative to the CG, it had the same source as the 1 Hz Y acceleration oscillation.

The largest discrepancies between the test and simulated rotation rates occur during the coasts after X thrust events. After the +X thrust event, the simulated Y and Z rotation rates show the effects of the geyser and subsequent slosh. These approach the test Y and Z rotation rates as the slosh damps out. This, along with the acceleration comparison at this time, implies the simplified simulation overpredicted the magnitude of slosh, which makes sense considering the lack of baffles. Interestingly, the simulated and test X rotation rate show good agreement throughout the coast. The simulated and test rotation rates do not agree well after 140 s.

DFTO1 Detailed Simulation Results.

Figures 10-12 are plots of the DFTO1 detailed simulation accelerations compared to the test data in the Orion Body Frame at the OIMU2 origin. Because the test data is the same as in Figures 4-6, test data specific comments mentioned above will not be repeated for these figures.

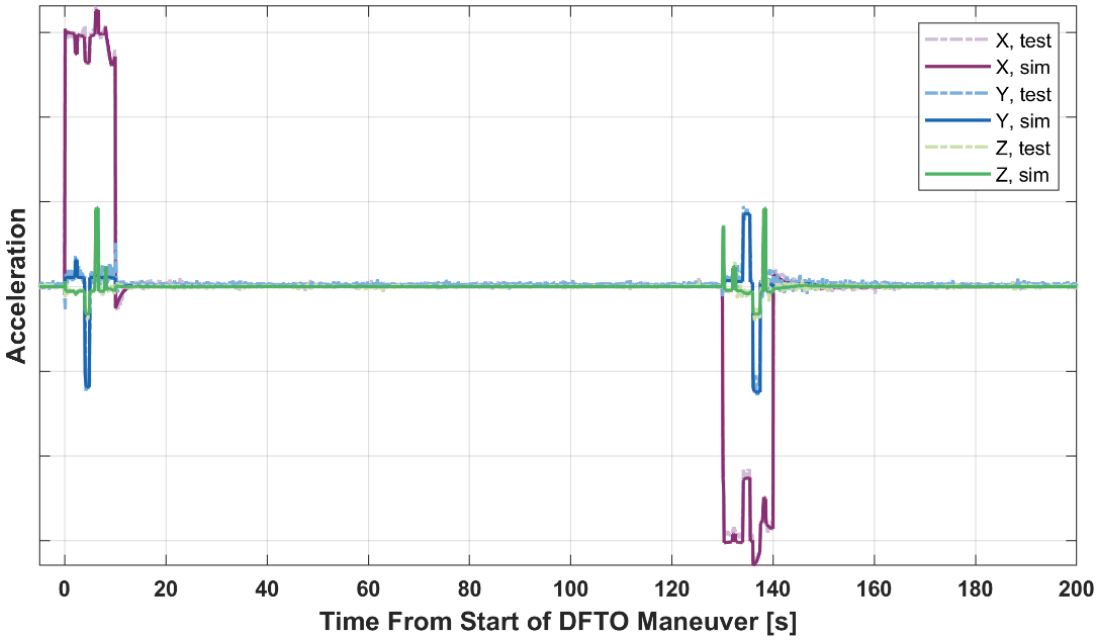

Figure 10. DFTO1 Detailed Simulation vs. Test Data: Accelerations

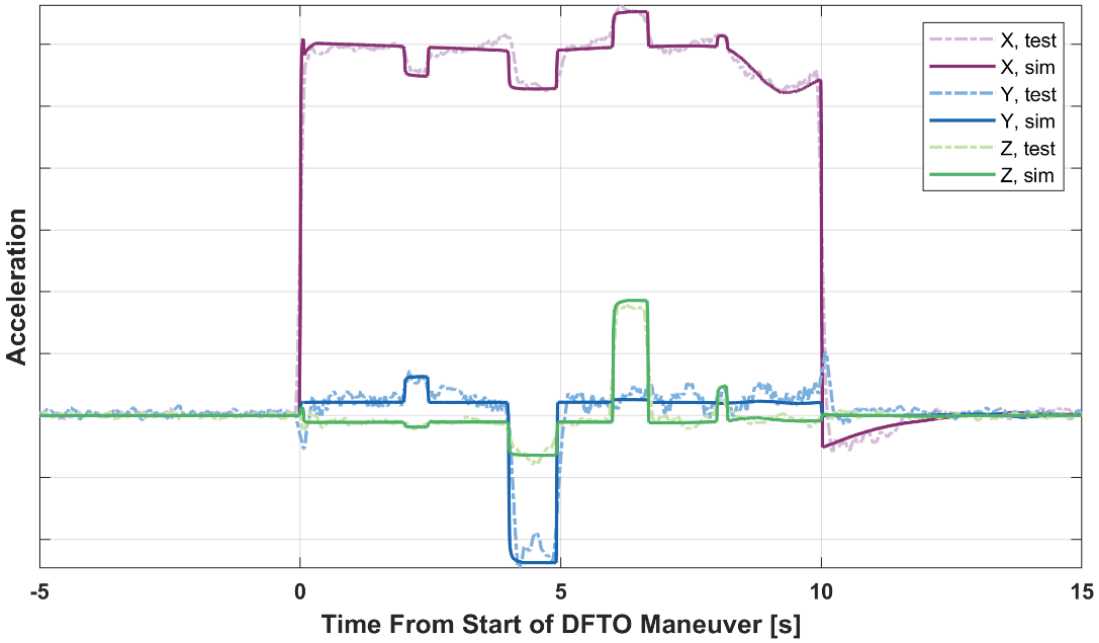

Figure 11. DFTO1 Detailed Simulation vs. Test Data: Accelerations, +X Thrust Event

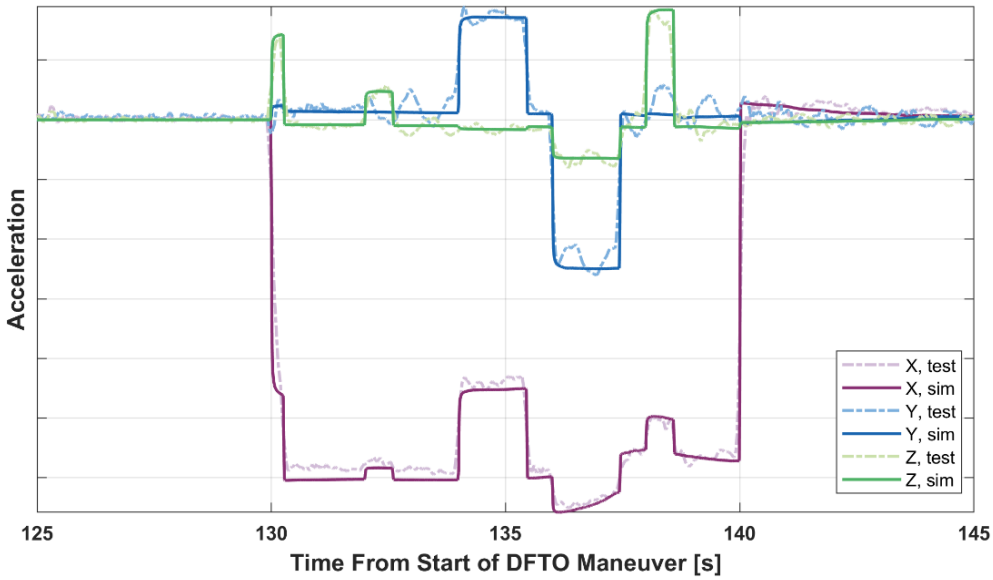

Figure 12. DFTO1 Detailed Simulation vs. Test Data: Accelerations, -X Thrust Event

Like the simplified simulation, the detailed simulation reproduced the rigid body motion effects well. The -Y bump at +X thrust initiation in Figure 11, +Y bump at +X thrust termination in Figure 11, and the roughly 1 Hz oscillation in the Y acceleration visible in Figures 11 and 12 were not seen in any simulations, which indicates that they were likely not from rigid body or slosh dynamics. The current best hypothesis is a solar array flex effect, though the main flex mode being less than 1 Hz (≈0.46 Hz) is contrary evidence.

Unlike the simplified simulation, the detailed simulation accurately reproduced the dip in X acceleration starting around 8 s and subsequent rise to 0 acceleration after 10 s, as shown in Figure 11. After the initiation of +X thrust, the simulation videos show an annular slosh wave traveling along each tank wall from the forward baffles towards the aft dome. The liquid clung to the walls due to surface tension, which is why the wave was annular rather than a single slug of liquid traveling down the tank axis. This wave entered the aft dome around 8 s, with the bulk of the wave having impacted by 10 s. The slosh wave arrival time was approximately 2 s faster than in the simplified simulation because it originated at the forward baffles instead of the forward dome, and, thus, had a significantly shorter distance to travel to the aft dome. Acceleration started trending up before thrust cutoff because the acceleration *decrement* due to -X slosh forces decreases. This confirms the hypothesis that this anomalous motion seen in the test was due to slosh. Unlike the simplified simulation, the detailed simulation included the AVB in the aft dome, which prevented geyser formation, resulting in better agreement with the test data after thrust termination. That said, the bulk propellants still obtained some +X motion, but not enough to have caused a noticeable acceleration.

The timing of the slosh events was slightly different between the two tanks due to their position in the ESM and differences in fluid properties; specifically, MMH tended to lag MON. The slosh proceeded to mostly damp out before the -X thrust event at 130 s (Figure 12), though it did not have time to reach the steady initial condition. Instead, the simulated liquid distribution at 130 s was more evenly distributed along the walls. The detailed simulation likely produced a more accurate propellant distribution at 130 s than the simplified simulation, resulting in motion after 130 s that agrees better with the test data. The -X thrust accelerates the liquid that is in the aft dome at 130 s towards the forward dome, mostly along the tank walls. Because the liquid was not concentrated in the aft dome, it did not form a distinct slosh wave as it did for the +X thrust event; instead, the migration to the forward dome was more continuous. The forward liquid motion damps out after thrust termination at 140 s, and Figure 12 simulation X acceleration shows a decrease from small positive acceleration to 0 during this time. It is difficult to distinguish from noise, but the X acceleration in the test data also appears to have the same trend after 140 s.

Figures 13-16 are plots of the DFTO1 detailed simulation rotation rates compared to the test data in the Orion Body Frame.

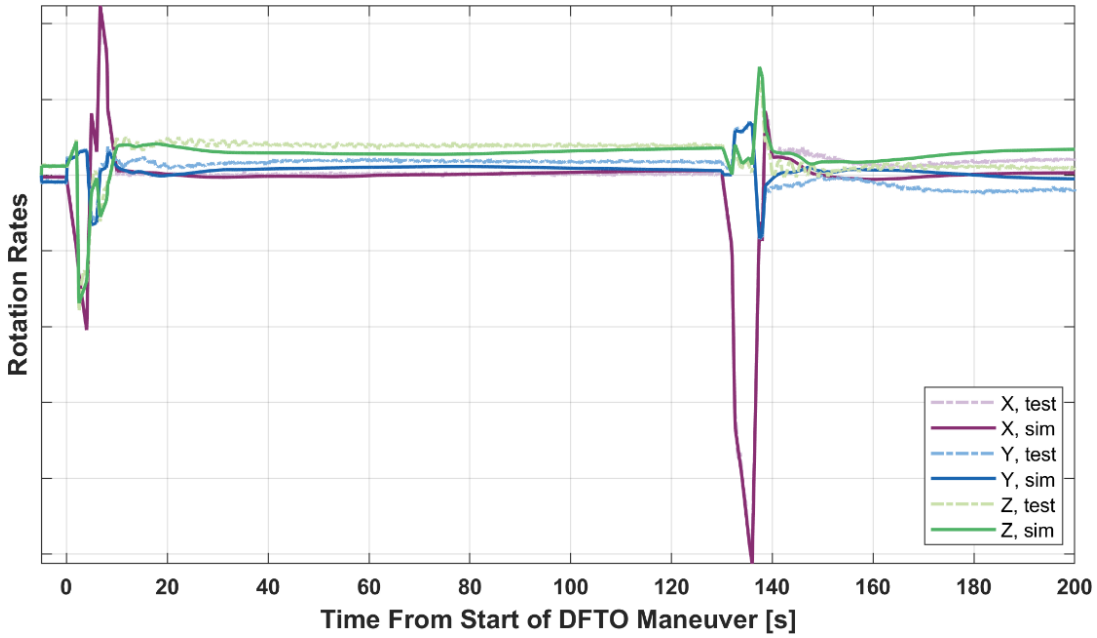

Figure 13. DFTO1 Detailed Simulation vs. Test Data: Rotation Rates

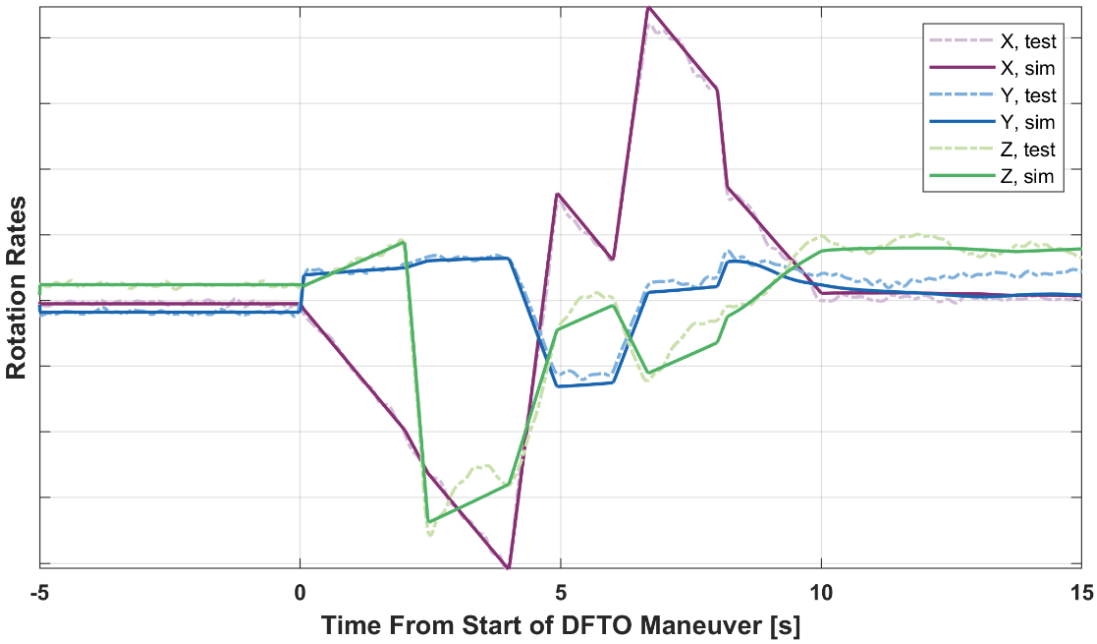

Figure 14. DFTO1 Detailed Simulation vs. Test Data: Rotation Rates, +X Thrust Event

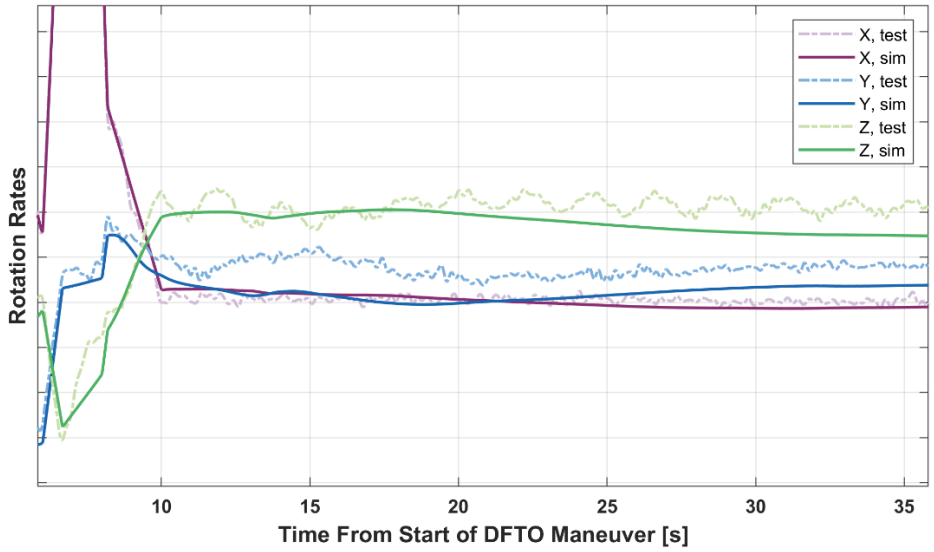

Figure 15. DFTO1 Detailed Simulation vs. Test Data: Rotation Rates after +X Thrust Event

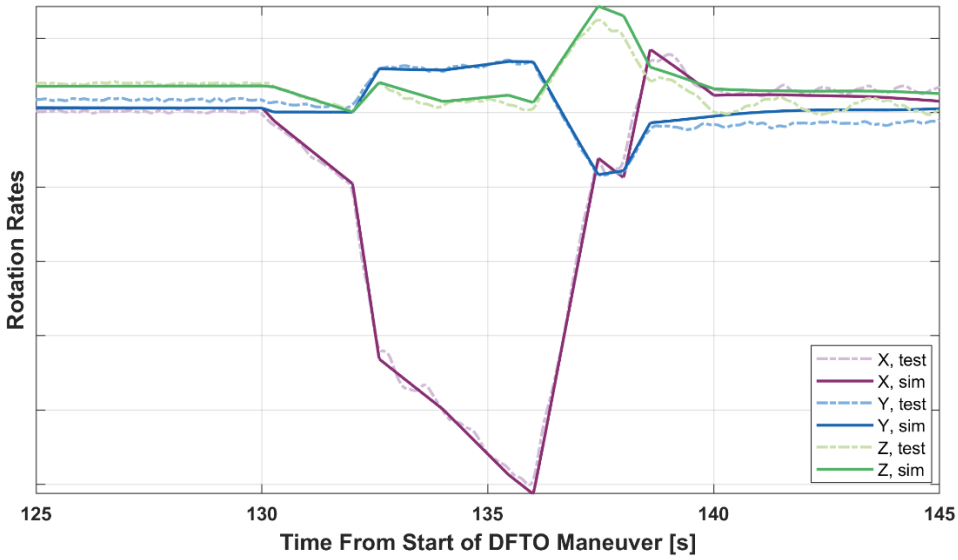

Figure 16. DFTO1 Detailed Simulation vs. Test Data: Rotation Rates, -X Thrust Event

The detailed simulation's rotation rates generally agree with the test data better than the simplified simulation. The slosh effects on the rotation rates were smaller than for the simplified simulation because the AVB prevented geyser formation. However, the AVB caused significant tank wall-directed splashing, which resulted in some minor Y and Z moments between 10-20 s. The Y and Z test data curves in Figure 15 show a couple slosh-moment-induced inflections between 10-20 s, with the higher frequency solar array flex mode superimposed. This effect was reproduced by the CFD, but the timing and rotation rate magnitudes slightly were off, with Z rotation rate agreeing better with test data than Y. The largest discrepancies between the test and simulated rotation rates occur during the coast after the -X thrust event, likely due to transient error growth.

As expected, the solar array flex mode visible in the Z rotation rate test data was not reproduced by the simulation. This mode is responsible for the test data Z rotation rate humps above the simulation Z rotation rate around 3, 5.5, and 7 s in Figure 14. There is an approximately 1 Hz mode visible in the X rotation rate

test data in Figure 16 that was also not reproduced by the simulation; the cause of this is unknown, but given the location of OIMU2 relative to the CG, it has the same source as the 1 Hz Y acceleration oscillation.

DFTO1 Bond and Weber Numbers.

Eqs. (1) and (2) define the Bond and Weber numbers. The accelerations at the tank geometric centers is more representative of the acceleration the fluid in the tanks experience than the body or OIMU2 accelerations, so they were used to calculate the transient Bond number. The test accelerations were transformed using Eq. (5) from the OIMU2 origin to the tank geometric centers. This required differentiating angular velocity to obtain angular acceleration, which increased noise. The simulation body accelerations were transformed from the CG to the tank geometric centers. These transformations were done in MATLAB in post-processing. Figure 17 compares test and simulated Bo for both tanks for DFTO1.

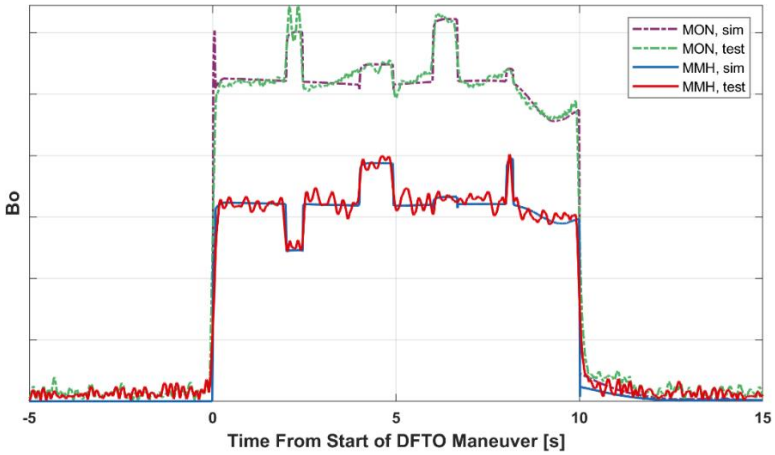

Figure 17. DFTO1 Bo, +X Thrust Event

The noise in the test Bo curves is apparent and worse than in the test acceleration and rotation rate curves due to the differentiation required to obtain angular acceleration. The tanks were on the lower side of the "high-G" Bo regime during thrust and in the low-G Bo regime during coast. Both tanks and thrust events had a small tail towards zero after thrust termination due to acceleration from slosh. The average test Bo during periods of no thrust was likely closer to 0 than shown because the acceleration magnitude squares each component of acceleration, which caused negative noise to become positive.

The velocity in the Weber number calculation was extracted from the simulations as the average speed of the fluid surface (isosurface of 0.5 volume fraction) relative to the tank walls. Since no fluid velocity measurement hardware was flown, We was not possible to calculate from the test data. Figure 18 compares the simplified and detailed simulations' We for both tanks for DFTO1.

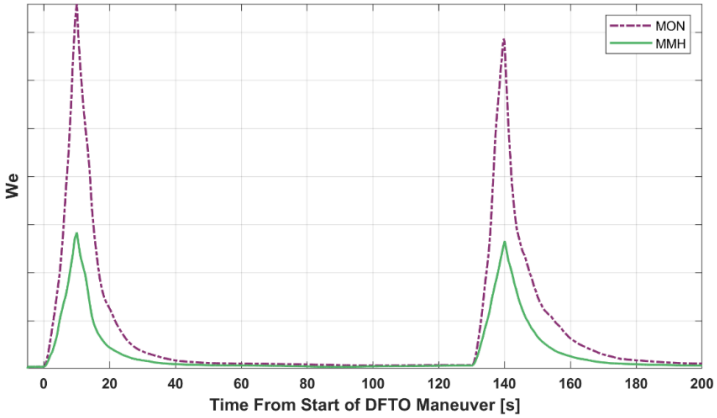

Figure 18. DFTO1 We

Peak We occurred at the end of the burns. MMH's higher surface tension and lower density resulted in a slightly lower average fluid surface speed than MON, but the majority of the difference in We is due to the difference in their densities. After thrust termination, the fluid speed decreases in time as the slosh damps out.

The tanks began in a surface-tension-force-dominated microgravity regime (Bo < 1 and We < 1). The tanks entered an acceleration-dominated high-G regime (Bo > 100, low We) at the start of a thrust event. As the fluids gained momentum, they transitioned to a roughly balanced acceleration and inertial forces regime (Bo > 100, We > 100). After thrust termination, Bo rapidly dropped below 30, while We remained high, resulting in the tanks being in a low-G inertial-force-dominated regime. Finally, the tanks returned to a surface-tension-force-dominated microgravity regime once the slosh damped out. The detailed simulation was able to accurately simulate slosh throughout all regimes.

CONCLUSIONS

The primary findings of this work are:

1. The hypothesis that the anomalous X acceleration signals around the time of X thrust termination were due to slosh is confirmed.
2. The slosh wave timing predicted by CFD simulations run during the slosh DFTO maneuver planning and subsequently used for timing the X thrusters was wrong, resulting in the slosh wave impacting while the X thrusters were still firing. This happened in DFTO1 because that CFD incorrectly predicted the initial condition of the propellants after the free-drift (centered ullage bubble) because it did not account for the surface tension effects of the internal baffles in the upstream tanks. The baffles in the forward half of the tank held a large portion of the propellant that would have been in the forward dome with no baffles present. Because the baffles are aft (-X) of the forward dome, the transit time of a slosh wave originating from there to the aft dome is less than from the forward dome to the aft dome. Thus, the slosh wave impacted the aft dome several seconds earlier than originally predicted. The detailed simulation in this work correctly predicted the initial condition and subsequent slosh.
3. Free-drift prior to a slosh maneuver does **not** guarantee a known fluid initial condition. The upstream tanks at the fill levels tested for DFTO1 had one minimum surface energy liquid configuration, but the DFTO2 tanks at the fill levels tested for DFTO2 had many.
4. Orion rotation rates are sensitive to Body Y and Z CG variations within their uncertainties. In other words, the uncertainties are relatively large, and a CG correction was necessary for both slosh DFTOs.
5. Accurate, individual thruster performance specifications are necessary for low-G coupled motion-slosh model validation similar to this. Modeled thrust changes on the order of 1% had a significant impact on overall motion of the vehicle over the time of the maneuver, and, therefore, the slosh excitation.
6. Low-G coupled motion-slosh CFD has been successfully validated using the Orion slosh DFTO test data. This is tempered by the fact that no tank camera was available, so there is no video of the actual slosh to compare to the simulation slosh videos. The validation is purely via the effects of the slosh on the spacecraft's motion.

There were three major test data features that were likely not noise, not due to rigid body or slosh dynamics, and could not be attributed to solar array flex. There is a -Y acceleration bump at +X thrust initiation, a +Y acceleration bump at +X thrust termination, and a roughly 1 Hz oscillation in the Y acceleration and X rotation rate that were not reproduced in any simulations. It is possible that these are due to solar array flex, but precisely how eludes the author. Any insight into these discrepancies would be appreciated.

Given the level of uncertainty in the mass properties, specifically Y and Z CG, uncertainty in the test data from noise, and how well the current detailed simulations agree with the test data, it is difficult to justify further improvements to the simulation methodology. Nevertheless, there are some potential improvements.

A finer mesh on the walls could resolve the fluid film that is likely present in microgravity. Alternatively, using adaptive mesh refinement around the fluid surface would increase surface tension accuracy without the expense of refining the entire mesh. The addition of flexible members to model the solar arrays could be beneficial given the fact that some of the solar array effects were of a similar magnitude to the slosh. This is theoretically possible to do within STAR-CCM+ but would likely be more error prone than co-simulating a dynamics model external to STAR-CCM+ with STAR-CCM+ only simulating the slosh.

On-orbit slosh testing is still important and necessary for slosh model validation. Had a well-validated low-G slosh model existed prior to Artemis 1, the risk that led to the DFTOs could have been dispositioned via analysis without the need for expensive (in terms of man-hours) on-orbit tests. Ideal validation cases for low-G slosh models have: 1. clean low-G, 2. well-characterized initial conditions, 3. accurately measured motion, and 4. visualization and/or measurement of fluid location. The data set used in this work has clean low-G and accurately measured motion. The excited slosh was enough to generate a significant deviation from rigid body motion, which allows these tests to be useful for slosh model validation without visuals or direct measurements of the fluid. Future on-orbit slosh tests should consider settling the propellants to one end of the tank so that the initial condition of the liquid is known more precisely. Some simulations were run with the simplified tank geometry and rotation initiated by a pitch moment, which showed significant sloshing from "flinging" the propellant across the tank. Given the success of the axially-excited slosh tests and CFD validation, future on-orbit slosh tests should consider exciting slosh with rotations instead of repeating X-axis tests. This has the additional advantaged of using the less-noisy gyroscopes as the primary data source for observing slosh effects.

Future work includes running DFTO2 detailed simulations with more initial conditions to find the one that yields the best agreement with test data. Some DFTO1 and DFTO2 simulations may be re-run with improved RCS thrust estimates. A formal uncertainty analysis to quantify the uncertainty of the IMU data is also planned. A low-G slosh model validation case will be created by organizing and formatting all of the slosh DFTO data and information, as well as the CFD simulations from this work. This validation case will be made available to NASA researchers interested in validating low-gravity slosh models.

ACKNOWLEDGMENTS

This work was funded by the NESC, and LSP provided software licenses and computer hardware. Thank you to the NESC Low-G Slosh team: Tannen VanZwieten for managing us, Jing Pei for providing the rigid body Simulink results, Brett Starr, Liam Elke, Bill Benson, Brandon Marsell, and Ether Lee. Thank you to all of the people that made Artemis 1 successful. In particular, thank you to those who made the slosh DFTOs happen and helped gather the information necessary for performing this analysis, especially Rodolfo Gonzalez, Greg Loe, and Michael Cooper. Thank you to Paul Tol for his colorblind-friendly colormaps, which were used for all plots in this work.

NOTATION

a	Acceleration, m/s^2
$\boldsymbol{a}$	Acceleration vector
Isp	Specific Impulse, s
$\dot{m}$	Mass flow rate, kg/s
$\boldsymbol{r}$	Position vector
R	Tank Radius, m
t	Time, s
T	Thrust, N
V	Velocity, m/s
ρ	Density, kg/m^3
σ	Surface tension, N/m
$\boldsymbol{\omega}$	Angular velocity vector

REFERENCES

[1] F. Dodge, "The New "Dynamic Behavior of Liquids in Moving Containers"," SWRI, San Antonio, TX, 2000.

[2] M. D. Berglund, C. E. Basset, J. M. Kelso and J. Mishic, "The Boeing Delta IV launch vehicle --Pulse-settling approach for second-stage hydrogen propellant management," *Acta Astronautica*, vol. 61, no. (1-6), pp. 416-424, 2007.

[3] T. E. Strikwerda, J. C. Ray, D. R. Haley and D. J. OShaughnessy, "NEAR Shoemaker: Major Anomaly Survival, Delayed Rendezvous and Mission Success," in Annual Rocky Mountain Guidane and Control Conference, Breckenridge, CO, 2001.

[4] J. M. Storey, "Principles of Fluid Dynamic Similarity Analysis for Slosh Experiments (AAS-24-097)," in *46th Annual AAS Guidance, Navigation and Control Conference*, Breckenridge, CO, 2024.

[5] G. Loe, R. A. Gonzalez, A. M. Dukes and M. Begley, "Artemis I DFTO-EM1-14 Low-G Axial Slosh Characterization FltDyn-CEV-23-25," NASA Orion Flight Dynamics Team, not publicly available, Johnson Spaceflight Center, 2023.

[6] D. A. Fester and P. E. Uney, "SS/RCS Surface Tension Propellant Acquisition/Expulsion Tankage Technology Program, CR-140299," Martin Marietta, Denver, CO, 1974.

[7] Lockheed Martin, Orion Exploration Mission Simulation Data Book LM-ORN-0985 Rev 8, Not publicly available, 2022.

[8] Lockheed Martin, Orion Exploration Mission Simulation Data Book LM-ORN-0985 Rev 7, Not publicly available, 2021.

[9] B. Determann, "MPCV-ESM-Propulsion Performance Model Description MPCV-RIBRE-TN-0083," Airbus DS GmbH, 2016.

[10] Lockheed Martin, Orion Exploration Mission Simulation Data Book LM-ORN-0985 Rev 5, Not publicly available, 2018.

[11] N. Kamins and J. Kruger, Artemis I Mass Properties Report (Post-flight) – Liftoff through ICPS Separation following TLI, MPCV-MP-22-006, Lockheed Martin, not publicly available, 2022.

[12] J. Peraire and S. Widnall, "Lecture L25 -3D Rigid Body Kinematics," Fall 2008. [Online]. Available: https://ocw.mit.edu/courses/16-07-dynamics-fall-2009/419be4d742e628d70acfbc5496eab967_MIT16_07F09_Lec25.pdf. [Accessed 5 8 2024].

[13] R. Gonzalez and M. J. Cooper, "Artemis I Low G Slosh Deeper Look Inputs 7-14," NASA, not publicly available, 2023.

[14] Siemens, "STAR-CCM+ 2023.0001 18.06.007-R8," 2023.

[15] Cadence, "Pointwise V18.6R6".

[16] J. M. Storey, "Experiments and Simulations of Liquid Mass Gauging and Slosh Dynamics in Microgravity," FloridaTech, Melbourne, FL, 2023.

[17] Mathworks, "MATLAB R2021a," 2021.